Nanoscale

Accepted Manuscript

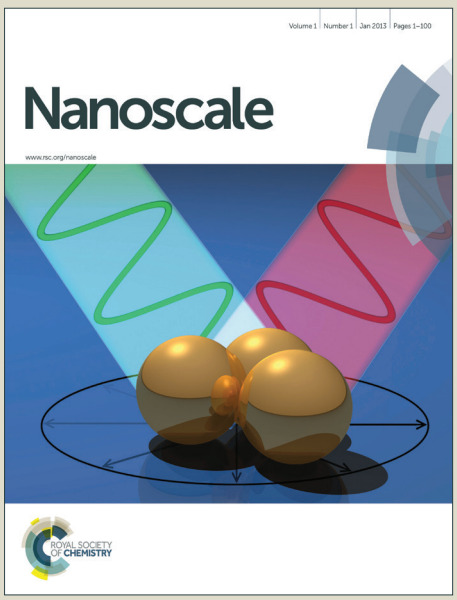

ROYAL SOCIETY OF CHEMISTRY

www.rsc.org/nanoscale

Cite this: DOI: 10.1039/c0xx00000x

www.rsc.org/xxxxxx

ARTICLE TYPE

Tessellated gold nanostructures from $Au_{144}(SCH_2CH_2Ph)_{60}$ molecular precursors and their use in organic solar cell enhancement

Reg Bauld[a], Mahdi Hesari[b], Mark S. Workentin[a,c] and Giovanni Fanchini[a,b,c]

Received (in XXX, XXX) Xth XXXXXXXXX 20XX, Accepted Xth XXXXXXXXX 20XX
DOI: 10.1039/b000000x

We report for the first time the fabrication of nanocomposite hole-blocking layers consisting of poly-3,4-ethylene-dioxythiophene:poly-styrene-sulfonate (PEDOT:PSS) thin films incorporating networks of gold nanoparticles assembled from $Au_{144}(SCH_2CH_2Ph)_{60}$, a molecular gold precursor. These thin films can be reproducibly prepared on indium tin oxide by spinning on it $Au_{144}(SCH_2CH_2Ph)_{60}$ solutions in chlorobenzene, annealing the resulting thin film at 400°C, and by subsequently spinning PEDOT:PSS on top. The use of our nanocomposite hole-blocking layers for enhancing the photoconversion efficiency of bulk heterojunction organic solar cells is demonstrated. Varying the concentration of $Au_{144}(SCH_2CH_2Ph)_{60}$ in the starting solution and the annealing time, different gold nanostructures were obtained, from individual gold nanoparticles (Au NPs) to tessellated networks of gold nanostructures (TessAu NPs). Improvement in organic solar cell efficiencies up to 10% relative to a reference cell is demonstrated with TessAu NPs embedded in PEDOT:PSS.

Introduction

Metallic nanoparticles (MNPs) have been utilized successfully to improve the performance of thin film solar cells.[1-4] Incorporation of MNPs into different components of photovoltaic devices can improve their light collection efficiency as well as their overall performance. In MNPs charge carriers collectively interact with incident photons at specific wavelengths corresponding to the plasmon resonance of the particles[4], which results in a strong interaction with light at specific frequencies. This interaction is highly dependent on the size and shape of the specific system of nanoparticles being considered.[4,5] The resulting enhancement of the local electric field in the proximity of the nanoparticles may lead to a higher absorption of incident light in a solar cell active layer located in the vicinity of MNPs. In addition, the increased optical cross section offered by MNPs of specific sizes may lead to an increased amount of light that can be scattered and trapped into the solar cell active layer.[6-8] Additional enhancements in solar cell performance are possible when MNPs are deposited directly onto the transparent conducting oxide thin film electrode of a solar cell. Transparent electrodes decorated with MNPs have resulted in an improved sheet conductivity[9] and, thereby, improved solar cell photoconversion efficiency[4, 10].

Several methods to incorporate metallic nanoparticles in thin film solar cells have been developed to date, which loosely fit in two categories. A first category, "top down" fabrication methods, relies on costly and time-consuming fabrication techniques, including optical and electron-beam lithography to pattern nanoscale metallic enhancement layers.[4] These methods provide the best control of the nanoparticle size and spacing and lead to relatively high performance enhancements. Conversely, a second category of techniques, "bottom up" methods, involves random growth of MNPs onto the requisite substrate by solution processing,[3,11] thermal evaporation of metallic thin films followed by thermal annealing, or other similar methods.[5] These approaches are more cost effective than "top down" methods, but distributions of particle shape, size, and spacing need to be carefully optimized in order to produce beneficial effects on the solar cell performance. Solution-processing techniques are promising methods for the incorporation of metallic nanoparticles into organic photovoltaics[12], but their effectiveness is still a matter of debate due to the difficulty in obtaining narrow distributions in particle size and a controlled patterning of MNPs.

In this paper, a novel, simple, and cost-effective solution-processing method to form systems of interconnected gold nanoparticles for plasmonic enhancement applications is presented. Nucleation is demonstrated at relatively low temperatures directly on indium tin oxide (ITO) thin films. $Au_{144}(SCH_2CH_2Ph)_{60}$, henceforth referred to simply as Au_{144}, is here utilized as the molecular gold precursor by first dissolving it in chlorobenzene and by subsequently spin-coating the resulting Au_{144} solution onto ITO-coated glass substrates. The sample is then annealed leading to the nucleation of Au_{144} molecules into tessellated systems of Au nanoparticles. These nanoparticles are of 5-40 nm in diameter, similar to what we previously observed for the nucleation of $Au_{25}(SC_2H_4Ph)_{18}$ molecular precursors in polyimide.[13] In addition, we are here presenting a method to independently control both the size and distribution of the resulting nanoparticles by independently changing two

parameters: the annealing time and Au_{144} concentration in the starting solution. Voronoi tessellation patterns of polystyrene nanoparticles on silicon are known to be attainable by exploiting spin-coating dynamics under specific conditions.[14] Here we demonstrate that the same method can also be used to control the nanoscale morphology of systems of MNPs and, specifically, gold nanoparticles, in ways that are not possible with conventional solution processing methods. Work by Yoon et al.[15] focused on depositing MNPs directly from solution. Although their method is relatively simple, it has far less control than ours over the specific MNP morphology. A significant benefit of using Au_{144} as a precursor for MNPs is in the large number of organic solvents that can be used for deposition. Consequently, a large variety of morphologies can be fabricated depending on the specific spin-coating dynamics involved. Specifically, Au_{144} and chlorobenzene as a solvent, we have been able to obtain for the first time Voronoi tessellation patterns from gold.

As a proof of concept of the relevance of our findings, we demonstrate our patterned gold layers in plasmonically enhanced Poly(3-Hexyl-Thiophene-2,5-diyl):[6,6]-Phenyl-C_{61}-Butyric acid Methyl ester (P3HT:PCBM) bulk heterojunction solar cells, in which they are incorporated in the hole-transport layer and demonstrated to overperform uniformly distributed gold nanoparticles (Au NPs). Consequently, our work indicates for the first time an avenue towards transferring molecular gold nanoclusters from the realm of fundamental chemistry and physics into practical applications in nanoplasmoniscs.

Experimental

Au_{144} molecules were synthesized by a modified Brust-Schiffrin method as reported elesewhere.[16] With this method, $HAuCl_4{:}3H_2O$ was dissolved in 50 mL water. Subsequently, 100 mL toluene containing 4.68 mmol of tetra-n-octylammonium bromide (TOABr) was added to the solution. The resulting salt was eventually transferred to the organic phase, which was then separated and cooled to 0 °C. Phenylethanethiol (19.4 mmol) was then added to the product, which was stirred for 3-hours until its color turned to an opaque white. At that point, 50 mmol (1.89 g) of sodium borohydride, dissolved in 30 mL of ice-cold water was added under vigorous stirring for 24 h. The resulting mixture was then repeatedly purified by solvent extraction using methanol and the purity of the product was checked using UV-visible spectrophotometry ,^{1}H nuclear magnetic resonance spectroscopy, as well as electrochemistry methods.[16 17]

A set of Au-NP decorated ITO thin films were prepared using the following methods. ITO-coated glass substrates (Aldrich cat no. 636916, 15-25 Ω/□ sheet resistance) were pre-cleaned in a bath sonicator using sequential detergent, acetone and methanol baths. Solutions of Au_{144} in chlorobenzene (PhCl) were subsequently spin-coated at 8000 rpm onto the ITO substrates. A set of samples was spin-coated by varying the concentration of Au_{144} in PhCl from 0.63 mg/mL to 5.00 mg/mL. This was done to study the effect concentration has on the resulting Au NP diameter and film morphology. These ITO thin films, with an Au_{144} layer spun on it, were all annealed for 9 min at 400 °C in air on a hot plate in order to nucleate the Au NPs. A second set of samples was prepared to study the effects of annealing time on the nucleation of Au NPs. This set of films was fabricated by annealing Au_{144} in air at times ranging from 9 min to 132 min at 400 °C while the concentration of the Au_{144}spin-coating solution in PhCl (5 mg/mL) was kept constant. All other spin-coating conditions were kept the same. A LEO (Zeiss) 1540XB Scanning Electron Microscope (SEM) operating at 10 keV was used to record electron microscope images of the samples. Energy-Dispersive X-ray (EDX) spectra were recorded with the same SEM instrument in order to verify that the nanoparticles were actually pure gold.

Two sets of solar cells utilizing a P3HT:PCBM bulk heterojunction architecture were prepared in order to demonstrate that our Au-NP decorated ITO thin films can lead to an enhancement in solar cell photoconversion efficiency. Thermal annealing of ITO at 400 °C and more is well known to induce structural, optical, and electrical changes in indium-tin oxides[18,19]. Consequently, the reference cell was treated by annealing the ITO layer to match the structural and optical changes undergone while forming the Au-NP layer. The first cell architecture (henceforth called TessAu-NP) featured an Au_{144} layer produced by spin-coating a 5.0 mg/mL solution of Au_{144} in PhCl directly onto ITO and then annealing in atmosphere at 400 °C for 132 min. A second type of cells (labeled as Au NP) were constructed by using a much thicker and continuous Au NP layer deposited by spin-coating at 1000 RPM from Toluene at 10 mg/mL concentration and then annealing at 400 °C for 10 min.

Each of the solar cells were prepared using the fabrication procedure described in detail in Ref. 20. Briefly, an electron-blocking, hole-transport layer consisting of a 30-nm Poly(3,4-Ethylene Di-Oxy-Thiophene):Poly-Styrene Sulfonate thin film (PEDOT:PSS, Aldrich cat no 483095) was spun at 3000 rpm from aqueous solution. The ITO films, with the PEDOT:PSS layer on the top of them, were introduced in a Nexus II dual glove box (Vacuum Atmospheres Co.) dedicated to organic solar cell fabrication and loaded with high-purity nitrogen, with oxygen and moisture levels less than 5 ppm. In this glove box, the ITO films coated with PEDOT:PSS were baked on a hot plate at 140°C for 30 min. The subsequent solar cell fabrication steps also occurred in the same glove box. The photovoltaic active layers were assembled by spinning on the top of PEDOT:PSS a 15:15 mg P3HT:PCBM solution in PhCl (Aldrich, cat no. 698989 and 684430, respectively). A spin-coating speed of 650 rpm, resulting in an active layer thickness of ~220 nm, was used. The resulting solar cells were then annealed at 120 °C for 15 min in the glove box and transferred, without direct exposure to air, into a contiguous high vacuum chamber with thermal evaporation facilities. The chamber was pumped down to ~10^{-7} Torr base vacuum. Ca/Al bilayer backing electrodes (20 nm Ca thickness and 80 nm Al thickness, measured by a Sycom STM-2 thickness monitor) were evaporated on each solar cell using a patterned shadow mask.[21] Each solar cell had the resulting device area of 0.245 cm^2. The resulting solar cell architectures are presented in Figure 5. Solar cell photoconversion efficiencies were determined from I-V curves measured directly in the glove box, using a Newport 9600 1.5 AM solar simulator at 1 sun. The solar simulator was calibrated using a Sciencetech SC-LT standard cell with certification accredited by the National Institute of Standards and Technology (ISO-17025). External quantum efficiency (EQE) measurements were performed outside the glove box using

a custom built apparatus[22] consisting of a 1000 W halogen lamp, a monochromator, and a calibrated photodiode.

Results and discussion

SEM characterization of samples of spun from solutions of Au_{144} at variable concentrations are shown in Figures 1a - 1d. We observe that both the size and distribution of the nanoparticles can be readily tuned by altering the concentration of Au_{144} in chlorobenzene. Varying the concentration from 0.625 mg/mL to 5.00 mg/mL gold nanoparticles with mean sizes between 5 nm and 30 nm were obtained in different samples. Resulting particle size distributions obtained at different concentrations of Au_{144} in PhCl are shown in Fig. 1e. Notably, samples prepared from PhCl solutions at higher concentrations of Au_{144} also exhibit more remarkable aggregation of the resulting gold nanoparticles.

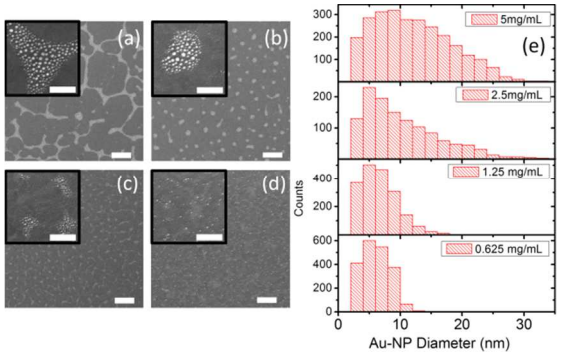

Figure 1: Inset images have a scale bar of 200 nm and large images have a 1 μm scale bar. SEM images of Au NP films nucleated from various concentrations of Au_{144} in solution. a) 5 mg/mL b) 2.5 mg/mL c) 1.25 mg/mL and d) 0.625 mg/mL. All samples were annealed at 400 °C for 9 min. (e) Particle size analysis on different samples. Higher concentration yield to TessAu-NP structures, as in panel a, while lower concentrations yield small clusters of nanoparticles. Very low concentrations appear to give an even distribution.

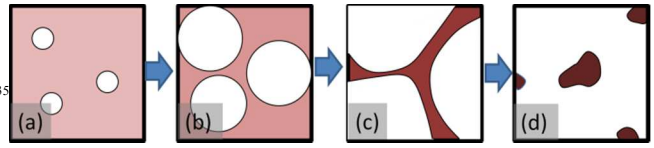

Figure 2: Diagram to show the process by which these films are deposited. a) Initial nucleation stage. Voids are created in the solvent film due to de-wetting. b) Voids continue to expand. c) Voids collide and can no longer expand. d) De-wetting continues and results in droplets. The remaining solvent is highly concentrated.

Figures 1a - 1d show that the networks of Au NPs on ITO obtained on these samples form web-like patterns that bear a good morphological resemblance to the structures described by Stange et al.[14] They found that under specific spin-coating conditions they can deposit interconnected networks of polystyrene. Stange et al show that such structures are a general result from rupturing of the solvent layer and the subsequent expansion of voids. This leads the polystyrene to form a connected network of polygons known as a Voronoi tessellation (compare Figure 1a with Figure 1d in Ref. 12). Due to the strong similarity between our Au-NP films and the polystyrene films of Stange et al and the similarity between the deposition methods we assert that the same physical processes underlie both of films. More recent work has been done to study these types of films in depth.[23, 24] The authors find that the interface between the solvent and the substrate strongly influences the resulting film morphologies and that the pattern formation process is driven by de-wetting and evaporation of the solvent. With this in mind we can understand how the different morphologies in figure 1 arise. We have outlined the process undergone during the deposition of these films in figure 2. Initially small voids form in the film due to spontaneous de-wetting, figure 2a. These voids then expand as shown in figure 2b until the voids collide as in figure 2c. During this entire process the concentration of Au_{144} in solution will be continuously rising due to the rapid evaporation of the solvent during spin-coating. Eventually the concentration of the Au_{144} reaches the saturation concentration of the solvent and will start precipitate out of the solution. They key to understanding how the different morphologies in figure 1 arise is to consider that the concentrations of the initial starting solutions is quite different. Therefore for different starting concentrations the saturation concentration will be reached at different times during the spin-coating process. The morphology in Fig 1a will result if the solvent reaches saturation concentration during the stage shown in Fig 2c as Au_{144} will start to precipitate while the "arms" shown in Fig 2c are still present. Continued de-wetting and solvent evaporation transforms the solvent into isolated droplets that result in the films seen in Fig 1b-c. The main difference between these films is that the droplets are allowed to reach smaller size before Au_{144} starts to precipitate. This then results in the smaller globules of Au-NPs that are observed and even the isolated nanoparticles that are observed in Fig 1d.

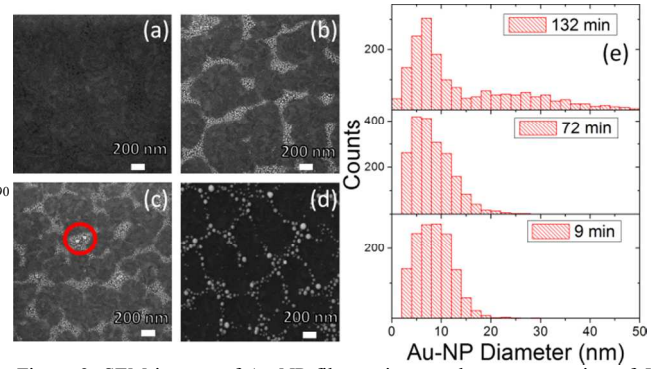

Figure 3: SEM images of Au NP films spin-coated at concentration of 5 mg/mL and then annealed at 400 °C for times up to 132 min. a) Pre-annealed state b) 9 min. annealing c) 72 min annealing, d) 132 min annealing. Highlighted is a cluster of NPs coalescing into a larger particle. Longer annealing times lead to TessAu NPs. e) Particle size distributions were measured on the SEM images.

In order to understand the processes occurring during the nucleation of the Au nanoparticles, the Au_{144} films were examined by SEM before and after thermal annealing at 400 °C. Figure 3a shows the films spun from 5 mg/L solution of Au_{144} in its pre-annealed state. The Au_{144} film (Figure 3a) deposits in much the same way as the resulting nanoparticles obtained after annealing (Figure 3b). This indicates that the micron scale morphology is due to spin-coating dynamic effects, as discussed above. It is therefore apparent that annealing times as short as 9 min. are sufficient to induce a complete transformation from an

assembly of Au_{144} molecules on ITO to a corresponding assembly of AuNPs. Longer annealing times permit an increase in the size of the nanoparticles by allowing more time for surface diffusion of Au atoms. This may be explained in terms of a statistical Ostwald ripening process,[25] for which larger particles grow at the expense of the smaller, because they are more thermodynamically stable due to lower surface energies. Small Au NPs will tend to coalesce into larger NPs given a sufficiently long annealing time. This process is observed in Fig 3c where we have highlighted a pair of small nanoparticles combining into a larger nanoparticle.

Compositional analysis of AuNP decorated ITO films was performed using EDX in order to estimate the purity of the AuNPs. Au_{144} molecular nanoclusters consist of 60 sulphur atoms per 144 Au atoms.[26] This gives an S/Au atomic ratio of 0.41. EDX measurements on our films show that S/Au = 0.36±0.01 indicating a slight sulphur deficiency in our films. This indicates that not every Au_{144} cluster is completely covered in thiol groups. After annealing EDX spectra of our samples show faint sulphur related peaks, with a nearly undetectable S content in most samples, as demonstrated in Figure 4. The reduction in sulphur content upon annealing can be explained by noting that the sulphur to gold bond is not stable at temperatures higher than 160 °C in an oxidizing environment.[27] Hence we expect that at temperatures of 400 °C in air the S bond will be oxidized following by subsequent evaporation of the thol group.

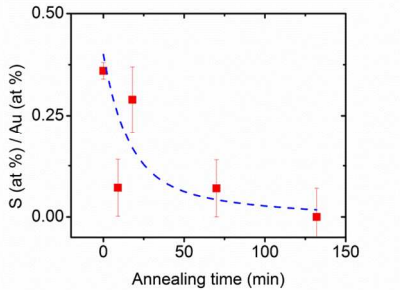

Figure 4: Ratio of S atomic % to Au atomic percent as measured by EDX. Initially there is a high S content. Annealing, even at short times removes most of the S from the NPs with the quantity being barely detectable under longer annealing times. . Blue line is a stretched exponential fit of the data.

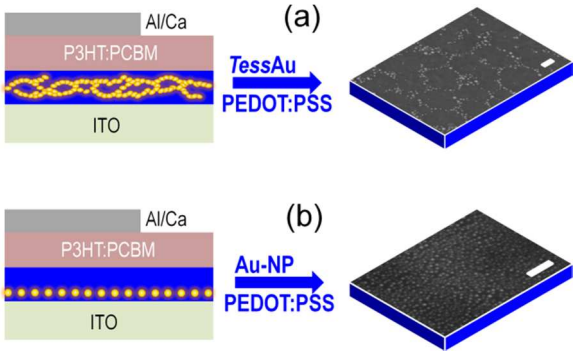

Figure 5: Diagram showing the solar cell architectures used in this work a) using tessellated gold nanoparticles in PEDOT:PSS fabricated by spin-coating 5 mg/ml of Au_{144} in ClPh and annealing for 132 min. b) Individual gold nanoparticles in PEDOT:PSS fabricated by spin-coating 10 mg/ml of Au_{144} in toluene and annealing for 10 min. Scale bars in the SEM images on the right are 200 nm.

Different sets of bulk heterojunction organic solar cells were fabricated to determine if these Au NP films can be used as an plasmonic enhancement layer. Figures 5a and 5b show the solar cell architecture and the SEM images of the gold-PEDOT:PSS nanocomposite hole-transport layers utilized in the two solar cells incorporating gold nanostructures assembled from Au_{144}. The first solar cell (panel a) utilizes a network of TessAu NPs at 5 mg/mL concentration in PhCl annealed for 132 min at 400 °C. The second solar cell (panel b) utilizes uniform layers of Au-NPs fabricated by spin-coating 10 mg/ml of Au_{144} in toluene and annealing for 10 min at 400 °C.

Table I – Series resistance (R_{series}), open circuit voltage (V_{oc}), short circuit current density (J_{sc}), fill factor and AM 1.5 photoconversion efficiencies (η) for the optimized solar cells studied in the present work compared to a reference cell with a PEDOT:PSS layer not containing gold nanoparticles.

	R_{series} (Ω)	V_{oc} (V)	J_{sc} (mA/cm^2)	Fill factor (%)	η (%)
TessAu-NP PEDOT:PSS	78±0.5	0.60±0.01	6.98±0.07	56.9±1.2	2.36±0.08
Au-NP PEDOT:PSS	174±1	0.53±0.01	3.5±0.04	47.2±0.9	0.88±0.04
Reference	91±0.5	0.59±0.01	6.82±0.07	53.7±1.0	2.14±0.07

Current-voltage curves of the solar cells under AM 1.5 illumination are displayed in figure 6 with additional information shown in Table 1. The Au-Tess cell yields J_{sc}=6.98±0.07 in comparison the reference cell has J_{sc}=6.82±0.07 for an overall increase in J_{sc} of 2.3%. In contrast in the Au-NP/PEDOT cell there is a reduction in I_{sc} of 51%. There are two competing factors that must be considered to understand the differences in these cells. First, that the local surface plasmonic resonance (LSPR) is concentrated strongly around the particle. The extension of the field enhancement is typically only a few nanometres.[28] Therefore the nanoparticle needs to be in close contact with the active layer to produce an enhanced absorption effect. When the AuNPs are placed below the PEDOT:PSS layer the LSPR field can decay significantly before reaching the active layer. It is therefore important to optimize the thickness of the PEDOT:PSS layer to achieve the best field enhancement. In our solar cells PEDOT:PSS films of approximately 30 nm were utilized. In this cell the Au-NPs used are 10 nm in diameter as seen in figure 5b. Therefore the LSPR has likely decayed before reaching the active layer and we expect the AuNP cell will yield a small or negligible LSPR enhancement. Indeed Yoon el al[15] have constructed similar devices using 5 nm Ag nanoparticles. They report an negligible change in J_{sc} when a MNP layer is deposited below the PEDOT:PSS layer. When the same MNPs are deposited on top of the active layer they then report an increase in J. This effect can also cause an increased optical absorption in the PEDOT:PSS layer which can further reduce the amount of available light collected in the active layer. The second factor involved is exciton quenching at the donor/acceptor interface. Work by Fung et al.[28] has shown that large concentrations of AuNP's has a detrimental effect on J_{sc} by way of exciton quenching. The interface between PEDOT:PSS and P3HT:PCBM gets increasingly rough and then results in a reduced J_{sc} by way of exciton quenching at the donor/acceptor interface.

In contrast, our Au-TessNP cell shows a slight improvement in

J_{sc}. In figure 3d-e, we can observe that the Au-TessNP films include larger MNPs, between 20 - 50 nm in size, in addition to ensambles of smaller nanoparticles of ~10 nm diameter. Smaller nanoparticles may have a detrimental effect on the overall device efficiency. As discussed by Fung et al.[28] a high density of small nanoparticles incorporated into the PEDOT:PSS layer can result in a decrease in J_{sc}. However, in our Au-TessNP solar cell, small MNPs are present at an overall density that is much lower than in the solar cell with uniformly distributed Au NPs.

Figure 6b shows the dark I-V curves of the Au-TessNP cell. The cell with the Au enhancement layer shows a slightly lower series resistance (R_s= 78±0.5 Ω) in comparison to the corresponding control cell (R_s = 91±0.5 Ω) calculated by taking the slope of the dark I-V curve at 0.8 V bias voltage. Since the equivalent circuit of a solar cell consists of a current source in parallel with a diode and a shunt resistor we can estimate the series resistance of the cell from the slope of the I-V curve taken above the diode turn on voltage. The improved series resistance indicates that the tessellated Au-NP layer is improving the electrical characteristics of the ITO contact in addition to the optical effects. Random distributions of MNPs can also have this effect, but the interconnected nature of these nanoparticle networks provide percolating conductive pathways that yield a significant improvement in sheet conductivity. This decrease in series resistance then leads to an improvement in fill factor, increasing from 53.7±1.0 % to 56.9±1.2 %. Combined with the improved J_{sc} we find a total improvement of solar cell efficiency from 2.14±0.07 % to 2.36±0.08 for an increase of 10.2 %.

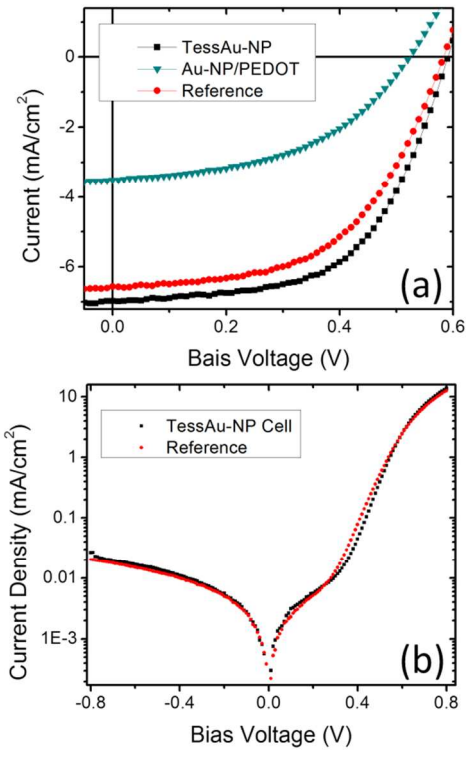

Figure 6: I-V curves of the prepared solar cells. a) I-V Curves under illumination. b) I-V Curve of TessAu-NP cell measured in the dark.

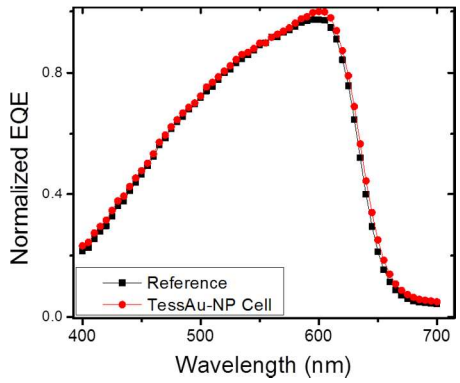

Figure 7: Normalized EQE showing an increase due to an enhanced light trapping in the solar cell utilizing a TessAu-NPs:PEDOT:PSS nanocomposite hole-transport layer. A redshift of the EQE spectrum is also noticeable for this device.

EQE measurements were performed on the solar cells that showed a net improvement in cell efficiency. These are shown in Figure 7. The enhanced solar cell shows a small increase in the measured EQE across almost the entire spectrum, with the largest improvement showing around ~620 nm. The plasmonic resonance peak of the AuNP films typically rests at around ~530 nm[29] so an enhancement indicates that the plasmonic resonance peak has possibly shifted due to a change in dielectric environment as the Au Nps are imbedded in PEDOT:PSS. Additionally there is a redshift in the EQE data that shows a more efficient collection of light at higher wavelengths further suggesting a plasmonic enhancement.

In conclusion, a simple way to fabricate an interconnected Au NP network by utilising the solvent deposition dynamics of a $Au_{144}(SCH_2CH_2Ph)_{60}$ clusters dissolved in chlorobenzene is demonstrated. The fact that Au_{144} clusters are soluble in many halogenated and aromatic organic solvents, such as chlorobenzene and toluene, gives them a wide range of possible uses as a AuNP precursor in comparison to precursors that can only dissolve in aqueous solution such as $HAuCl_4.3H_2O$. The utility of these films as a plasmonic enhancement layer in organic solar cells was also demonstrated as they yield a 10% improvement in cell efficiency when incorporated into the PEDOT:PSS layer. Future work will focus on better understanding how all the different morphologies presented in this paper influence thin film organic solar cells.

[a] *Department of Physics and Astronomy, University of Western Ontario, London, Ontario N6A 3K7, Canada. Fax: 519-661-2033; Tel: 519-661-2111 ext. 86238; E-mail: gfanchin@uwo.ca*
[b] *Department of Chemistry, University of Western Ontario, 1151 Richmond St., London, Ontario N6A 5B7, Canada. Tel: (519) 661-2111 Ext 86319; E-mail: mworkent@uwo.ca*
[c] *Centre of Advanced Materials and Biomaterials Research (CAMBR), University of Western Ontario, 1151 Richmond St., London, Ontario N6A 5B7, Canada.*

‡ This work is supported through the Natural Sciences and Engineering Research Council of Canada (NSERC) Discovery Grant (DG) Program. GF acknowledges a Canada Research Chair in Carbon-based nanomaterials and financial support from the Canada Foundation for Innovation (CFI). RB acknowledges a NSERC Postgraduate Scholarship. This work was partially carried out at theWestern University Nanofabrication Facility.

1. D. Derkacs, S. H. Lim, P. Matheu, W. Mar and E. T. Yu, *Appl Phys Lett*, 2006, **89**.
2. Y. S. Hsiao, S. Charan, F. Y. Wu, F. C. Chien, C. W. Chu, P. L. Chen and F. C. Chen, *J Phys Chem C*, 2012, **116**, 20731-20737.
3. F. C. Chen, J. L. Wu, C. L. Lee, Y. Hong, C. H. Kuo and M. H. Huang, *Appl Phys Lett*, 2009, **95**.
4. H. A. Atwater and A. Polman, *Nat Mater*, 2010, **9**, 205-213.
5. S. Eustis and M. A. El-Sayed, *Chem Soc Rev*, 2006, **35**, 209-217.
6. H. A. Atwater and A. Polman, *Nat Mater*, 2010, **9**, 205-213.
7. J. L. Wu, F. C. Chen, Y. S. Hsiao, F. C. Chien, P. Chen, C. H. Kuo, M. H. Huang and C. S. Hsu, *ACS Nano*, 2011, **5**, 959-967.
8. J. Yang, J. You, C. C. Chen, W. C. Hsu, H. R. Tan, X. W. Zhang, Z. Hong and Y. Yang, *ACS Nano*, 2011, **5**, 6210-6217.
9. C.-S. Hong, H.-H. Park, J. Moon and H.-H. Park, *Thin Solid Films*, 2006, **515**, 957-960.
10. K. Nakayama, K. Tanabe and H. A. Atwater, *Appl Phys Lett*, 2008, **93**, -.
11. S. Maenosono, T. Okubo and Y. Yamaguchi, *J Nanopart Res*, 2003, **5**, 5-15.
12. J. L. Wu, F. C. Chen, Y. S. Hsiao, F. C. Chien, P. L. Chen, C. H. Kuo, M. H. Huang and C. S. Hsu, *ACS Nano*, 2011, **5**, 959-967.
13. R. Bauld, M. Hesari, M. S. Workentin and G. Fanchini, *Appl Phys Lett*, 2012, **101**.
14. T. G. Stange, R. Mathew, D. F. Evans and W. A. Hendrickson, *Langmuir*, 1992, **8**, 920-926.
15. W. J. Yoon, K. Y. Jung, J. W. Liu, T. Duraisamy, R. Revur, F. L. Teixeira, S. Sengupta and P. R. Berger, *Sol Energ Mat Sol C*, 2010, **94**, 128-132.
16. R. L. Donkers, D. Lee and R. W. Murray, *Langmuir*, 2004, **20**, 1945-1952.
17. J. F. Hicks, D. T. Miles and R. W. Murray, *J Am Chem Soc*, 2002, **124**, 13322-13328.
18. Y. L. Hu, X. G. Diao, C. Wang, W. C. Hao and T. M. Wang, *Vacuum*, 2004, **75**, 183-188.
19. S. H. Wang, Y. J. Hsiao, T. H. Fang, S. L. Chen and S. H. Kang, *Microsystem Technologies*, 2013.
20. R. Bauld, L. M. Fleury, M. Van Walsh and G. Fanchini, *Appl Phys Lett*, 2012, **101**.
21. A. Gupta, V. Armel, W. C. Xiang, G. Fanchini, S. E. Watkins, D. R. MacFarlane, U. Bach and R. A. Evans, *Tetrahedron*, 2013, **69**, 3584-3592.
22. M. S. Ahmed, PhD Thesis, University of Western Ontario, 2013.
23. S. H. Choi and B. M. Z. Newby, *Surf Sci*, 2006, **600**, 1391-1404.
24. X. Han, J. Hu, H. L. Liu and Y. Hu, *Langmuir*, 2006, **22**, 3428-3433.
25. P. W. Voorhees, *J Stat Phys*, 1985, **38**, 231-252.
26. O. Lopez-Acevedo, J. Akola, R. L. Whetten, H. Gronbeck and H. Hakkinen, *J Phys Chem C*, 2009, **113**, 5035-5038.
27. Z. K. Wu and R. C. Jin, *ACS Nano*, 2009, **3**, 2036-2042.
28. D. D. S. Fung, L. F. Qiao, W. C. H. Choy, C. D. Wang, W. E. I. Sha, F. X. Xie and S. L. He, *J Mater Chem*, 2011, **21**, 16349-16356.
29. J. H. Lee, J. H. Park, J. S. Kim, D. Y. Lee and K. Cho, *Org Electron*, 2009, **10**, 416-420.